Upper Devonian mercury record from North America and its implications for the Frasnian–Famennian mass extinction

Liu, Zeyang; Percival, Lawrence; Vandeputte, Delphine Jenny; Selby, David; Claeys, Philippe; Over, Jeffrey; Gao, Yue

Published in:
Palaeogeography, Palaeoclimatology, Palaeoecology

DOI:
10.1016/j.palaeo.2021.110502

Publication date:
2021

License:
CC BY-NC-ND

Document Version:
Accepted author manuscript

Upper Devonian mercury record from North America and its implications for the Frasnian–Famennian mass extinction

Zeyang Liu[1,2,3], Lawrence M. E. Percival[4], Delphine Vandeputte[4], David Selby[3,5], Philippe Claeys[4], D. Jeffrey Over[6], Yue Gao[4]

[1]State Key Laboratory of Organic Geochemistry, Guangzhou Institute of Geochemistry, Chinese Academy of Sciences, Guangzhou 510640, China

[2]CAS Center for Excellence in Deep Earth Science, Guangzhou, 510640, China

[3]Department of Earth Sciences, University of Durham, Durham DH1 3LE, UK

[4]Analytical, Environmental and Geochemistry Group, Vrije Universiteit Brussel, Pleinlaan 2, 1050 Brussels, Belgium

[5]State Key Laboratory of Geological Processes and Mineral Resources, School of Earth Resources, China University of Geosciences, Wuhan, 430074, Hubei, China

[6]Department of Geological Sciences, SUNY College at Geneseo, Geneseo, NY 14454, USA

Corresponding author: Zeyang Liu (geozy.liu@outlook.com)

Lawrence M. E. Percival (Lawrence.Percival@vub.be), Delphine Vandeputte (Delphine.Jenny.Vandeputte@vub.be), Philippe Claeys (phclaeys@vub.be), D. Jeffrey Over (over@geneseo.edu), Yue Gao (Yue.Gao@vub.be)

Abstract

The Frasnian–Famennian biotic crisis (~372 Ma) was one of the "big five" mass extinction events in the Phanerozoic. This event was associated with dramatic climatic and oceanographic perturbations, including oceanic anoxia, global cooling, sea-level fluctuations, etc. Large-scale volcanic activity is one of several possible triggers that have been suggested as the ultimate cause of this crisis, based on Hg enrichment data from widespread sections. However, there are also sections that do not show a Hg enrichment across the Frasnian–Famennian boundary. To further investigate the hypothesis of a volcanic trigger for the Frasnian–Famennian mass extinction event, mercury (Hg) analyses were performed on six North American records (five from the Appalachian Basin and one in the Illinois Basin) that include the Frasnian–Famennian boundary. There is no uniformly observed Hg enrichment at or below the Frasnian–Famennian boundary across the six sites. A potentially volcanically driven Hg anomaly is found in the Illinois basin; however, the Hg enrichment occurs stratigraphically above the Frasnian–Famennian boundary. Mercury records from the studied sites question the timing of the volcanism that may be responsible for the mass extinction event. Further studies are needed to fully understand the geographic distribution and eruption history of the large igneous provinces, as well as the link between Hg and volcanism during the Frasnian–Famennian interval.

Keywords: Appalachian basin; Illinois basin; volcanism; large igneous provinces; wildfires

1. Introduction

The Late Devonian Frasnian–Famennian (F–F) mass extinction (also known as the Upper Kellwasser Crisis, ~372 Ma; Becker et al., 2012; Da Silva et al., 2020; Percival et al., 2018a), is one of the 'big five' mass extinction events of the Phanerozoic Eon (Stanley, 2016). Marine ecosystems, especially metazoan reefs, were severely impacted during this biotic crisis (Ma et al., 2016; Stanley, 2016). Stratigraphic records of the extinction are associated with a large positive carbon-isotope excursion (up to 4 ‰) both in the inorganic and organic carbon contents ($\delta^{13}C_{carb}$ and $\delta^{13}C_{org}$) of sedimentary strata in the *linguiformis* conodont Zone (= Frasnian Zone 13b) across the globe, indicating perturbations to the carbon cycle beginning ~150 kyr prior to the end of the Frasnian Stage (e.g., Chen et al., 2005; De Vleeschouwer et al., 2017; Joachimski and Buggisch, 1993; Joachimski et al., 2002; Stephens and Sumner, 2003; Wang et al., 1996). Proposed causes of the F–F mass extinction event include globally anoxic or euxinic marine conditions (Bond et al., 2004; Song et al., 2017), land-plant evolution (Algeo et al., 1995), climate cooling (Huang et al., 2018; Joachimski et al., 2009; Joachimski and Buggisch, 2002), sea-level change (Bond and Wignall, 2008; Johnson et al., 1985), bolide impact (Claeys et al., 1992) and volcanism (e.g., Racki, 2020; Racki et al., 2018b). Recently, the volcanism scenario has been supported by the discovery of spikes in mercury (Hg) concentrations at several F–F boundary records (Estrada et al., 2018; Moreno et al., 2018; Racki et al., 2020; Racki et al., 2018a; Racki et al., 2018b; Kaiho et al., 2021). Mercury and its isotopes have been used as a marker of ancient

62 volcanic events associated with several other major climate perturbations and/or
63 extinctions in the geological history, such as the Permian–Triassic mass extinction,
64 Toarcian Ocean anoxic event, Late Ordovician mass extinction, Paleocene–Eocene
65 thermal maximum, and end-Devonian mass extinction, etc. (e.g., Grasby et al., 2016;
66 Grasby et al., 2020; Grasby et al., 2013; Grasby et al., 2017; Grasby et al., 2019; Jones
67 et al., 2018; Liu et al., 2019a; Percival et al., 2018b; Percival et al., 2015; Paschall et
68 al., 2019; Sanei et al., 2012; Shen et al., 2019a; Shen et al., 2019b; Them et al., 2019;
69 Kaiho et al., 2020, 2021). Volcanic events can emit mercury through two pathways: (1)
70 direct outgassing from effusive and explosive volcanic eruptions, and (2) Hg-enriched
71 volatiles that are hypothesized to have been generated by contact metamorphism of
72 organic-rich sedimentary rocks and subsequently emitted through hydrothermal vent
73 complexes (Jones et al., 2019). In either case, the emitted Hg is distributed far from the
74 source through the atmosphere, due to a relatively long stratospheric residence time of
75 around 0.5–2 years (e.g. Driscoll et al., 2013). In modern environments, mercury is
76 typically deposited to sediments complexed with organic matter (Gamboa Ruiz and
77 Tomiyasu, 2015; Gehrke et al., 2009; Outridge et al., 2007; Sanei et al., 2014). Thus,
78 normalization against TOC is necessary to evaluate whether any Hg enrichment is
79 caused by increased organic matter preservation or an externally derived influx of the
80 element during perturbations of the local/global Hg cycle. In addition to organic matter,
81 clay minerals and sulphides may also be important host fractions within the sediments
82 (Grasby et al., 2019; Shen et al., 2019a, 2020). However, in spite of global-scale records

of Hg enrichment at the Frasnian–Famennian boundary, some sections do not show a trend of Hg enrichment (Racki et al., 2019). Thus, the timing and magnitude of the volcanism that may be responsible for the Frasnian–Famennian biotic crisis is still poorly understood.

In addition to volcanism, local/global Hg cycling may also be perturbed by the disruption of terrestrial Hg sources, such as wildfires and continental runoff (e.g. Amos et al., 2014; Biswas et al., 2007; Sanei et al., 2012; Them et al., 2019; Grasby et al., 2017; Shen et al., 2019c). Forests and organic-rich upper soils are major terrestrial Hg pools (e.g., Obrist et al., 2018); thus, biomass burning would release Hg back into the atmosphere and volatile Hg that stored in organic-rich soils (Obrist et al., 2018). The amount of Hg released from wildfire would, of course, depend on the quantity of plant burning to some degree. The burning severity is also an important factor controlling the degree of Hg emission from wildfires (Webster et al., 2016). The higher the burning temperature, the greater the emissions of Hg from soil heating (Webster et al., 2016). It has also been suggested that Hg emissions from post-fire soil erosion could represent a significant Hg source to the oceans and atmosphere (Melendez-Perez et al., 2014).

Finally, terrestrial runoff can also act as an important contributor to the Hg budgets of the oceans (Fisher et al., 2012; Soerensen et al., 2012). The majority of Hg is bound to organic matter particles in the river and deposited in deltas, estuaries and on the continental shelf (Chester, 1990). Thus, riverine Hg discharges largely affect nearshore Hg sediments, as supported by the Hg-isotopic compositions of nearshore *vs* more distal

marine sediments (e.g., Grasby et al. 2017; Shen et al., 2019). In the event of enhanced continental weathering, riverine Hg input to the ocean would likely become more significant (Grasby et al., 2017; Them et al., 2019). Although wildfires and riverine Hg inputs are relatively well constrained in the modern Hg cycles (e.g., Amos et al., 2014; Obrist et al., 2018), their role in ancient Hg records are still poorly understood due to both a paucity of data (but see Grasby et al., 2017; Them et al., 2019), and, in the case of the Devonian, a markedly different global paleogeography and terrestrial biosphere.

In this study, we perform mercury (Hg) analysis on six Frasnian–Famennian boundary sections from North America (New York and Iowa). We discuss the potential evidence for volcanic and terrestrial mercury emissions at the time of the Frasnian–Famennian extinction, and, by inference, any potential volcanic link with that biotic crisis. Of the investigated sections, the five New York sites comprise a proximal to distal transect, and have been previously examined for wildfire records (Liu et al., 2020a). As such, these sections are also ideal for the evaluation of wildfires and riverine runoff (as well as volcanism) as sources of Hg input into the oceans in the geological record.

2. Geological background

In this study, samples were collected from six Frasnian–Famennian archives of North America (Fig. 1). Five records from western New York were investigated, including four outcrop sections (Joint Creek, JC; Beaver Meadow Creek, BMC; Irish Gulf, IG; Walnut Creek Bank, WCB), and one drill core (West Valley, WV). These

125 records are preserved as slope to basin deposits from the northern Appalachian foreland
126 basin, and are interpreted as proximal to distal deposits in terms of paleoceanography,
127 with the following order of increasing distance from the paleoshoreline: JC, BMC, WV,
128 IG and WCB (see inserted map of Fig. 1) (Over et al, 1997, 2002; Sageman et al., 2003).
129 In all five records, the studied interval is composed of the latest Frasnian–earliest
130 Famennian Hanover Formation and the early Famennian Dunkirk Formation. The
131 Hanover Formation is dominated by light gray, silty shales (less than 1 wt. % total
132 organic carbon, TOC) interbedded with black silty shales that is rich in organic matter
133 (~1–6 wt. % TOC) with low thermal maturity (BR_o ~ 0.6 %, solid bitumen reflectance;
134 Liu et al., 2020a). The grey shales are bioturbated, and poorly preserved brachiopods
135 and bivalves have been identified within it (Over, et al., 1997; Over, 2002). The black
136 shales are rich in pyrite and finely laminated (except the base parts where bioturbation
137 is observed), suggested that they were deposited in anoxic/dysoxic conditions (Lash,
138 2017; Over, et al., 1997; Over, 2002; Sageman et al., 2003). The Hanover Formation is
139 overlain by the Dunkirk Formation, which contains thick beds of black shale (Over, et
140 al., 1997). In all five Appalachian Basin records studied here, the F–F boundary is
141 defined by the first occurrence of the conodont *Palmatolepsis triangularis* (Fig. 2;
142 Klapper et al., 1993; Over, 1997, 2002). This boundary occurs in a regionally
143 continuous bed of black shale that is thought to locally mark the Upper Kellwasser
144 Horizon (Over, 1997, 2002).

To obtain a more regional scale viewpoint beyond the local environment of the Appalachian Basin, the H-32 drill core was studied as a sixth record, consisting of sediments deposited in a deep-water environment of the Illinois Basin (40.47° N, 91.47° W; Fig. 1; Day and Witzke, 2017). The Frasnian–Famennian interval in the Illinois Basin is composed of the Sweetland Creek Shale Formation (shales and carbonates) and the overlying Grassy Creek Shale Formation (fissile organic-rich brown shale). The F–F boundary is positioned just above the base of the Grassy Creek Shale (above the conodont Zones 13b and 13c; i.e., the *linguiformis* interval) (Fig. 3; De Vleeschouwer et al., 2017). Several volcanic ash layers are also preserved in the lowermost part of Grassy Creek Shale Formation, just above the F–F boundary (Fig. 3; De Vleeschouwer et al., 2017).

3. Methods

Mercury (Hg) concentrations were determined on an Advanced Mercury Analyser (AMA) 254.7 at Vrije Universiteit Brussel. Mercury in the solid sample was volatilized during direct thermal decomposition of the sample, and the resultant gas drawn into an amalgamator containing a gold trap, before being analyzed by atomic absorption spectrometry (see Sholupov and Ganeyev, 1995). Blank measurements on the AMA during the analyses were better than 0.001 ng. 100±2 mg of powdered sample was used per analysis, with at least two measurements per sample to check repeatability, which was typically better than ±10%. The accuracy and repeatability of the measurements

was further tested by multiple measurements of the Certified Reference Material IAEA-MESL-ILC-TE and an internal sedimentary sample SCH U5 as standards.

Total organic carbon (TOC) contents and isotopic compositions of the TOC were determined for samples from the H-32 core using a Nu Instruments Horizon 2 coupled to an Eurovector isotope ratio mass spectrometer (IRMS) elemental analyzer EuroEA3000 at the Vrije Universiteit Brussel (Belgium). Approximately 1–2 grams of homogenized powder were decarbonated with 10% HCl, before being rinsed three times with mill-Q water and dried at 50 °C. Analyses of the decarbonated samples were calibrated using the international reference materials IAEA-CH-6 (sucrose), and multiple certified reference materials that have been calibrated against international standards: IA-R041 (L-alanine), IVA33802151 (organic-rich sediment), IVA33802153 (organic-poor soil). The measured carbon content in decarbonated powder was converted to a bulk rock TOC value by accounting for the measured mass lost following decarbonation. Analytical uncertainty was typically better than ±0.1 wt% (1σ) for carbon contents, and ±0.2 ‰ (1σ) for isotopic compositions.

4. Results

All the Hg analysis data are listed in Table S1 and S2, and the stratigraphic plots are presented in Fig. 2 and Fig. 3.

At the Joint Creek section, the Hg concentrations are generally above 30 ppb below the F–F boundary, dropping slightly to ~25 ppb at the base of the Dunkirk Formation. The Hg/TOC values show a slight increase from ~20 ppb/wt.% at the

bottom part to ~26 ppb/wt.% towards the F–F boundary, which then decrease to ~20 ppb/wt.% at the base of Dunkirk Formation.

At the Beaver Meadow Creek section, the Hg values are generally about 20 ppb in the lower part of the section, with an increase up to ~54 ppb about 15 cm below the F–F boundary. The Hg values then drop to ~30 ppb immediately below the boundary and further decline to ~20 ppb across it. Hg/TOC values also reach their maximum about 15 cm below the F–F boundary (from ~10 to ~22 ppb/wt.%), dropping to less than 10 ppb across the F–F boundary.

At the West Valley section, the Hg values range from ~22 to 43 ppb across the studied intervals, with no clear pattern observed. The Hg/TOC values average about 35 ppb/wt.% (n = 6) at the lowest part of the section, which then decrease gradually to about 11 ppb/wt.% around the F–F boundary and remain at ~10 ppb/wt.% up section, except for one sample with an anomalously high Hg/TOC value (81.88 ppb/wt.%) that is caused by low TOC level (0.32% compared to average 2.5% for adjacent samples).

At the Irish Gulf section, the Hg values drop from ~30 ppb to 15 ppb at the very bottom part, which then rapidly increase to ~46 ppb around the F–F boundary. The Hg values then decrease to about 25 ppb and further drop slightly to about 23 ppb upwards. The Hg/TOC values drop gradually from ~12 ppb/wt.% to ~5 ppb/wt.% across the F–F boundary and remain around 5 ppb/wt.% towards a higher stratigraphic level.

At the Walnut Creek Bank section, the Hg values increase from ~35 ppb to ~56 ppb across the F–F boundary, which then gradually drop to ~25 ppb at the base of the

206 Dunkirk Formation. Except for a very high Hg/TOC value of 51 ppb/wt.% at the bottom
207 of this section, samples below the F–F boundary generally have Hg/TOC values about
208 11 ppb/wt.%, which then gradually decrease to ~6 ppb/wt.% towards the lower part of
209 the Dunkirk Formation (Fig. 2).

210 In the H-32 core, the Hg values range from ~44 to 213 ppb (average ~98 ppb, n =
211 19), with several peaks at the bottom part of the section, which then gradually decrease
212 to a minimum of ~16 ppb just below the F–F boundary. The Hg values then increase
213 sharply to ~314 ppb immediately above the F–F boundary, before gradually declining
214 to ~46 ppb at the top of the studied interval. A minimum threshold of 0.2 wt.% TOC
215 has been suggested for normalization of Hg by TOC, in order to avoid artificially
216 inflated Hg/TOC spikes due to the high uncertainty/value ratio of the TOC data (Grasby
217 et al., 2016). A sharp rise in TOC content takes place just below the F–F boundary,
218 from typically <0.5 wt.% (apart from a discrete layer between 281–335 cm where
219 values rise to over 2 wt. %), to an average of 3.1 wt.% in the uppermost Frasnian and
220 Famennian strata (Fig. 3). This rise in TOC occurs at the base of the Grassy Creek Shale
221 Formation and within a broad rise in $\delta^{13}C_{org}$ values from -28.5 ‰ to -27.1 ‰, and is,
222 therefore, interpreted as marking the local expression of the Upper Kellwasser Horizon.
223 The Hg/TOC values average about 251 ppb/wt.% (n = 16) at the lower part of the
224 section, with two one-point excursions to 790 and 722 ppb/wt.%. The Hg/TOC values
225 then drop to ~200 ppb/wt.% below the F–F boundary, which then further drop to ~17
226 ppb/wt.% across the F–F boundary. A one-point excursion to 1127 ppb/wt.% is detected

above the F–F boundary, reflecting a low TOC value (0.2 %) of the sample compared to the rocks either side that feature both high Hg and organic matter contents (Fig. 3). Notably, both Hg and Hg/TOC values recorded in the H-32 core are significantly higher than for the five Appalachian Basin records.

5. Discussion

5.1 Constraining the Hg source(s)

The Appalachian Basin sites have Hg values average 30.5 ppb (15.1 ppb/wt.% Hg/TOC), which are relatively low compared to postulated average shale concentrations (62.4 ppb Hg and 71.9 ppb/wt.% Hg/TOC; Grasby et al., 2019). Thus, the majority of the samples (except the peaks in Hg documented from the H-32 core) would also be classified as average shale contents (Fig. 3). This low Hg abundance does not seem to result from dilution by a high sedimentation rate, as the formation of shale generally requires a low sedimentation rate, and there is no discernible Hg abundance difference between the WV and WCB sections where sedimentation rates could vary by up to ~7 times (based on an appropriate estimation according to the thickness between the F–F boundary and the base of the Dunkirk Formation). In addition to organic matter, the Hg may also be associated with sulphides and clay minerals in certain environments (Bergquist, 2017; Shen et al., 2019a; Shen et al., 2020; Them et al., 2019). Thus, if mercury is deposited bound to one of those phases, it may cause a rise in sedimentary Hg and Hg/TOC values without any major increase of the Hg fluxes from its sources. However, Algeo and Liu (2020) compiled a large geochemical dataset

248 of trace-metal redox proxies and found that the Hg/TOC and Hg/S ratios of ancient
249 sediments were generally not significantly related to local redox conditions, and thus
250 might reflect volcanic Hg fluxes. A non-relationship between redox changes and
251 Hg/TOC ratios is also supported for the sites studied here by the lack of correlation
252 between Hg/TOC and redox proxies (Mn, Mo, V/[V + Ni], Mo_{EF}, V_{EF} and Ni_{EF}; Table
253 S1).

254 After normalization against the TOC data, only the Beaver Meadow Creek section
255 from western New York shows a minor Hg (Hg/TOC) enrichment below the F–F
256 boundary. No positive correlation between this Hg peak and Mo concentrations is
257 observed; indeed, the increase of Hg and Hg/TOC values is associated with a decrease
258 in Mo content (Fig. 2 and 4, Table S1, $r = +0.10$, $p(a) > 0.05$, $n = 52$). The Mo element
259 might be affected by changes of the marine reservoir size due to restriction of the
260 Appalachian Basin (Algeo, 2004). However, Hg and Hg/TOC values also lack
261 correlations with Mn and V/(V+Ni) proxies (Fig. 4). This result suggests that the
262 mercury enrichment did not result from redox changes or a switch to burial with
263 sulphides. An increase of clay mineral content is also excluded for driving the Beaver
264 Meadow Creek Hg enrichment, as no liner relationship is observed between
265 sedimentary Hg and Al_2O_3 contents (Table S1; $r = +0.10$, $p(a) > 0.05$, $n = 52$).

266 Previous studies have suggested that wildfire activity could release Hg into the
267 environment (Biswas et al., 2007; Sanei et al., 2012; Them et al. 2019; Grasby et al.,
268 2017, 2019, and references therein). Fossilised charcoal, a by-product of wildfires, has

been widely used to study ancient fire events (e.g., Glasspool and Scott, 2010). A previous organic petrology study of the New York sections found the presence of fossilised charcoal (inertinite) as evidence for wildfire activity (Liu et al., 2020a). However, no correlation between Hg concentration and inertinite abundance is observed in this study (Fig. 2; Liu et al., 2020a). Although it is possible that wildfire-released Hg and charcoal (inertinite) entailed different durations to reach the depositional record, it would be expected that the majority of Hg and inertinite would be deposited geologically simultaneously. During biomass burning, Hg is released from plant combustion, as well as soil heating (Friedli et al., 2003; Obrist et al., 2007). Thermal volatilization of the Hg bonded to the organic-rich soil would occur at 150 °C (Biester and Scholz, 1996), with mercury readily emitted once the soil reached that temperature (Biswas et al., 2007, 2008; Woodruff and Cannon, 2010). Previous charcoal-reflectance analyses have suggested that the type of wildfire documented in the New York F–F records was surface fire, with a burning temperature between 400 and 500 °C (Liu et al., 2020a). The primary burnt material was herbaceous and shrubby plant matter (Liu et al., 2020a), and it is possible that such plants do not sequester Hg efficiently. However, previous research has suggested that the temperature of burning is different from that of soil heating due to a strong thermal gradient. Thus, a fire with burning temperature of 850 °C on the surface would generally not increase the subsurface temperature over 150 °C below 5 cm (Debano, 2000). If this was also the case for wildfires during the F–F extinction, it might explain the apparent lack of Hg

290 emissions from soil heating at that time. Alternatively, the wildfires may have been too
291 small in scale (with a low burning severity), or the ash and charcoal have too low a Hg
292 content, to supply large amounts of mercury to the local environment. Kaiho et al.
293 (2021) report Hg/TOC enrichments together with coronene spikes are shown for three
294 carbonate-dominated F-F sections (Yangdi, China; Sinsin, Belgium; Coumiac, France;
295 with TOC generally less than 0.3 %), and concluded that the Hg was emitted from
296 thermal heating of country rocks by sill intrusion, rather than normal wildfire, as
297 supported by the evidence of coronene index [coronene/(benzo[e]pyrene +
298 beozo[ghi]perylene + coronene)] (Kaiho et al., 2016, 2020, 2021). Whilst coronene
299 requires higher energy to form than other polycyclic aromatic hydrocarbons (PAHs), a
300 higher energy demand cannot rule out the wildfire origin of coronene. Additionally,
301 there are also further factors that may affect the PAHs compositions (e.g. burning
302 pattern, plant community etc.; Boudinot and Sepúlveda, 2020; Lima et al., 2005). In
303 addition, most samples have coronene index over the threshold of 0.2 in the studied
304 sections (which would suggest coronene generated from heating by sill intrusion or
305 wildfires set by high temperature magma, in contrast to normal wildfires, according to
306 the authors), and this would imply a prolonged time duration for the volcanism, which
307 is unlikely and does not correlate with the Hg/TOC profiles. We suggest that it is still
308 at an early stage to link the coronene spikes with magmatic activity and interpret the
309 Hg/TOC as a signal of volcanism and associated volatilization of mercury from
310 organic-rich sediments by sill intrusions. Importantly, other events for which sill

311 intrusions of organic-rich shales have been proposed invariably feature a pronounced
312 negative carbon-isotope excursion (assumed to reflect the large-scale release of
313 isotopically light carbon from the intruded lithologies; e.g., Svensen et al., 2004, 2009;
314 McElwain et al., 2005), in contrast to the positive $\delta^{13}C$ shift that marks the F–F
315 boundary.

316 Riverine discharge of Hg to the oceans is another important source and may
317 significantly affect the Hg record of the proximal sections (e.g., Amos et al., 2014 and
318 many others). In theory, if riverine input is the controlling factor of Hg enrichment, a
319 trend of decreasing Hg concentrations from proximal to distal transections might be
320 expected (see Them et al., 2019). However, no such relationship is found within the
321 five Appalachian Basin sections. Rather, the most distal sections have the highest
322 average Hg abundance (from proximal to distal: Joint Creek–29.5 ppb, Beaver Meadow
323 Creek–30.8 ppb, West Valley–29.7 ppb; Irish Gulf–28.1 ppb; Walnut Creek Bank–
324 35.32 ppb). We have also noted that the four proximal sections have very similar
325 average Hg concentrations, despite variable TOC amounts (from proximal to distal:
326 Joint Creek–1.37 %, Beaver Meadow Creek–2.33 %, West Valley–2.10 %; Irish Gulf–
327 3.40 %). As such, our data suggest that riverine Hg input and organic matter
328 sequestration played minimal roles in the Hg enrichment within the Appalachian Basin.
329 However, it is also possible that the studied sites are too geographically close to yield
330 any noticeable difference on the Hg records, as evidenced by similar Ti/Al values of
331 these sections (Fig. 1, Table S1).

Racki (2020) proposed a hypothesis of masked signal of Hg in Devonian records, i.e., a co-increase of productivity and Hg abundance may keep the Hg/TOC values constant, or even reduce the Hg/TOC values if the percentage increase of organic matter preservation is higher than the amount of Hg increase, as has also been proposed for some Mesozoic events (see Percival et al., 2015, 2018b; Charbonnier and Föllmi, 2017). However, for the western New York sites, increases in both Hg and Hg/TOC are largely absent, suggesting that there was no major increase in mercury input to this region, rather than a volcanic influx that was then masked by elevated TOC. The variations of the Hg data in western New York sections are more appropriately explained by a combination of local depositional factors. In summary, the western New York sections show no major perturbations of the Hg cycle that may be linked with volcanic events. Variations of local depositional factors are more likely to be the main control of the Hg fluctuations at western New York sections.

Two Hg/TOC spikes (up to ~800) are detected about 4–6 m below the F–F boundary in the H-32 core (Fig. 3). These Hg enrichments are well above the background the Hg/TOC values, suggesting a potential volcanic contribution or local environmental perturbation (e.g., sulphides depositions), although currently the exact roles of clay mineral and sulphides are not evaluated due to a paucity of data. However, these peaks are about 750–900 kyr before the mass extinction event (De Vleeschouwer et al., 2017). Consequently, even if those Frasnian Hg/TOC peaks are indicative of

large-scale volcanic eruptions, they likely occurred too early to have triggered the mass extinction event.

We have also noticed that both the H-32 core and the West Valley section express a single-point Hg/TOC peak above the F–F boundary (Fig. 2 and 3), although there is no evidence as to whether these enriched strata are time equivalent. However, these Hg/TOC spikes are not likely caused by enhanced Hg input from volcanism, due to their apparent correlation to a TOC minimum in those intervals (Fig. 2 and 3). The H-32 core does document large-scale Hg perturbations from less than 100 ppb to over 300 ppb above the F–F boundary, but the Hg/TOC values generally remain relatively constant. Thus, these strata could simply record an increase in organic matter burial under anoxic–euxinic conditions, and a resultant rise in Hg deposition. Intriguingly however, this increase in Hg content correlates with the lowermost Famennian volcanic ash layers preserved in the H-32 core (Fig. 3), potentially indicating volcanism as an Hg source that was muted by excess organic-matter deposition, (Fig. 3; cf. Racki, 2020). This scenario would match the model of Racki (2020), but even if this was the case, this volcanism occurred after the F–F extinction, and cannot have triggered the event.

5.2 No Hg evidence in North America for a volcanic trigger of the F–F mass extinction

A volcanic trigger has long been proposed to have caused the F–F mass extinction (e.g., Courtillot et al., 2010; Kravchinsky, 2012; Racki et al., 2002). Recently, this scenario has been supported by the discovery of widely distributed Hg anomalies in the

F–F stratigraphic interval (Estrada et al., 2018; Moreno et al., 2018; Racki et al., 2020; Racki et al., 2018a; Racki et al., 2018b), although some localities do not show a Hg enrichment signal (Racki et al., 2019). In this study, among the five sections investigated in western New York, only one section (Beaver Meadow Creek) expresses a Hg and Hg/TOC peak below the F–F boundary (Fig. 2), but it is too small in scale to be unequivocally linked with volcanism rather than local depositional processes, and may simply result from a combination of changes in local depositional environments, such as redox variation, organic matter preservation, sulphide precipitation and clay mineral input. The H-32 section in Iowa shows a major Hg enrichment (from 58 to 314 ppb), which is correlative with volcanic ash layers, but this Hg peak is above the F–F boundary (Fig. 2 and 3), and is largely correlative with elevated TOC contents. Even if the H-32 peak was associated with volcanism, it remains unclear whether it was linked to local eruptions that produced the ash layers, or a large-scale magmatic event (e.g., Viluy Traps, Kola, Vyatka, and Pripyat-Dniepr-Donets rift systems; Arzamastsev et al., 2017; Kiselev et al., 2006; Kravchinsky, 2012). However, a correlation between individual eruptive events and stratigraphic Hg enrichments has been speculated for other sites, and increased arc activity also postulated as a trigger for the F–F extinction (Racki et al., 2018; Racki, 2020).

The osmium-isotope ratio of a sedimentary rock is another widely used proxy to study ancient volcanic events (e.g., Dickson et al., 2015; Du Vivier et al., 2014; Georgiev et al., 2015; Liu et al., 2020b; Liu et al., 2019b; Percival et al., 2020; Peucker-

Ehrenbrink and Ravizza, 2012; Turgeon and Creaser, 2008). The modern seawater osmium-isotope ($^{187}Os/^{188}Os$) composition is controlled by the mass balance of unradiogenic Os input from mantle and extraterrestrial sources (~0.126) and riverine input of radiogenic material following weathering of ancient continent crust (~1.4 today) (Peucker-Ehrenbrink and Ravizza, 2000). In the event of large-scale volcanism and/or weathering of newly emplaced volcanic basalts, a shift in the Os-isotope profile to lower values would be expected (e.g., Du Vivier et al., 2014; Georgiev et al., 2015; Liu et al., 2019b; Turgeon and Creaser, 2008). However, available Os-isotope data for the F–F transition interval do not show a clear unradiogenic shift, although a few data points do have quite unradiogenic values of ~0.2 and 0.3 (Gordon et al., 2009; Liu et al., 2020a; Percival et al., 2019; Turgeon et al., 2007). Thus, if volcanism indeed occurred at this time, it is likely to be a small/transient event that differs from other LIPs claimed to be responsible for major environmental/biotic perturbations. For example, LIP activity associated with the Late Cretaceous Cenomanian–Turonian Oceanic Anoxic Event lasted ~200 kyr and is marked by a global-scale shift to very unradiogenic values in the sedimentary Os isotope record (e.g., Du Vivier et al., 2014, 2015; Percival et al., 2020; Jones et al., 2020). Prolonged unradiogenic Os isotope shifts are also documented in response to widespread igneous activity related to the Central Atlantic magmatic province during the Triassic–Jurassic boundary interval (Cohen and Coe, 2002; Kuroda et al., 2010).

Instead, an increase in Os isotope values has been reported from the Kowala Quarry section (Poland), and interpreted to reflect enhanced weathering of the continent (Percival et al., 2019). Although this same signal has not been reported from the New York Sites (Turgeon et al., 2007; Gordon et al., 2009; Liu et al., 2020a), it should be noted that those osmium records focus on the F–F boundary itself, whereas the Kowala weathering peak is just below the base of the Upper Kellwasser Level, which is typically somewhat stratigraphically below the F–F horizon, and thus may not have been reached by the New York datasets. However, a weathering signal in Os isotopes does not prohibit the occurrence of volcanic activity, if the influx of unradiogenic Os from volcanism was outweighed by radiogenic Os input from weathering of the continental crust, as is thought to be the case for the Toarcian Ocean Anoxic Event (Cohen et al., 2004; Percival et al., 2016; Kemp et al., 2020; Them et al., 2017), and potentially the PETM to some degree (Ravizza et al., 2001; Dickson et al., 2015).

Whilst not supported by the coronene index and the lack of a negative $\delta^{13}C$ excursion, sill intrusion is still a possible scenario that would leave the majority of igneous unit underground. Such a process could have allowed Hg to be emitted without exposing massive mafic rock onto the Earth surface that could have been weathered to deliver large amounts of unradiogenic osmium into the ocean (Dickson et al., 2015; Liu et al., 2019a; Wieczorek et al., 2013). An impact scenario has also been proposed for the F–F interval (e.g., Claeys et al., 1992). However, current Os isotope data do not show any unradiogenic excursion that may support an impact scenario, and even if an

435 impact event occurred, the impactor is likely to have a very small size that leaves little
436 geochemical trace in the sedimentary record (Harris et al., 2013; Liu et al., 2020a;
437 Percival et al., 2019; Turgeon et al., 2007). Further studies about the timing, locality
438 and scale of proposed large igneous provinces are needed to fully understand the role
439 of large igneous provinces in the climate change and mass extinction of Late Devonian.
440
441 *5.3 Implications for the link between volcanism and the F–F mass extinction*
442 Whilst volcanism has been inferred as the cause of the Frasnian–Famennian mass
443 extinction on the basis of Hg spikes at several sections around the world, it is clear that
444 these enrichments are not documented in all locations (Estrada et al., 2018; Moreno et
445 al., 2018; Racki et al., 2020; Racki et al., 2018a; Racki et al., 2018b; Kaiho et al., 2021;
446 this study), arguing against a global-scale disturbance of the mercury cycle. Even where
447 Hg spikes are preserved, there is no consistency regarding their stratigraphic correlation.
448 Mercury enrichments are detected below, at and above the F–F boundary (e.g., Kaiho
449 et al., 2021; Racki, 2020 and references therein, H-32 core in this study). In addition,
450 several LIPs (e.g., Viluy Traps, Kola, Vyatka, and Pripyat-Dniepr-Donets rift systems;
451 Arzamastsev et al., 2017; Kiselev et al., 2006; Kravchinsky, 2012) were active during
452 the F–F period. Thus, even if the previously observed Hg anomalies were derived from
453 volcanism, it remains unclear whether they were sourced from a single volcanic system
454 or a combination of the LIPs, or an intensification in arc volcanism.

Further studies are needed to rigorously test the link between Hg and volcanism during the F–F interval, especially the relative timing of sedimentary Hg enrichment and F–F mass extinction (see e.g., Percival et al. 2018a). Moreover, high-resolution geochronology work that can precisely characterize the eruption/magmatic history of the LIPs is necessary to fully understand the role of volcanism in driving the climatic and biotic changes during the F–F period (following the approaches undertaken for the P–T mass extinction and Siberian traps, and T–J mass extinction and Central Atlantic Province; e.g., Burgess et al., 2017; Davies et al., 2017).

6. Conclusions

Mercury records of six Upper Devonian sections from North America show no sign of Hg enrichment associated with the F–F mass extinction (Fig. 2 and 3). Minor Hg variations in the New York records are more likely to be controlled by a combination of local deposition processes such as redox variation, organic matter preservation, sulphide precipitation and clay mineral input, rather than perturbations by volcanic events. Previous study of the New York sections suggests enhanced wildfire activity (as evidenced by inertinite abundance) across the F–F interval. The lack of correlation between inertinite abundance and Hg concentration data excludes wildfires as a major source of Hg during the F–F transition interval, at least to North American basins. These findings may indicate that during the F–F extinction, ash and charcoal had low Hg contents, or that the wildfires were limited in scale and/or had low burning

severity that released minimum Hg into the local environment. The H-32 section (Iowa) records a possible volcanism-driven Hg enrichment with coeval increase of TOC values; however, this Hg anomaly is stratigraphically above the F–F boundary (Fig. 3). A volcanic trigger for the F–F mass extinction has recently been supported by Hg anomalies data from widespread localities, but is not reinforced by study of the North American F–F archives investigated here. Further investigations are needed to understand why some F–F records are marked by pronounced Hg peaks, and others not, as well as the timing and scale of Late Devonian volcanism and its potential role in driving the F–F biotic crisis.

Acknowledgements

We thank Jin Si Over for field assistance in collecting the New York outcrop sections. Brian Slater at the New York State Museum is thanked for facilitating the collection of the WV core samples, and Jed Day and the Iowa Geological Survey for access to the H-32 core. David Verstraeten and Christophe Snoeck are thanked for assistance with laboratory analyses. We gratefully acknowledge the TOTAL Endowment Fund and the CUG Wuhan Dida Scholarship to DS, the Flanders Research Foundation (FWO: grant no 12P4519N), and Vrije Universiteit Brussel to LMEP and the University of Durham, China Scholarship Council, China Postdoctoral Science Foundation and Guangzhou Institute of Geochemistry to ZL.

References

497 Algeo, T.J., Berner, R.A., Maynard, J.B., Scheckler, S.E., 1995. Late Devonian oceanic
498 anoxic events and biotic crises:“rooted” in the evolution of vascular land plants.
499 GSA today 5, 45.
500 Algeo, T.J., 2004. Can marine anoxic events draw down the trace element inventory of
501 seawater? Geology 32, 1057-1060.
502 Algeo, T.J., Liu, J., 2020. A re-assessment of elemental proxies for paleoredox analysis.
503 Chemical Geology 540, 119549.
504 Amos, H.M., Jacob, D.J., Kocman, D., Horowitz, H.M., Zhang, Y., Dutkiewicz, S.,
505 Horvat, M., Corbitt, E.S., Krabbenhoft, D.P., Sunderland, E.M., 2014. Global
506 Biogeochemical Implications of Mercury Discharges from Rivers and Sediment
507 Burial. Environmental Science & Technology 48, 9514-9522.
508 Arzamastsev, A.A., Vesolovskiy, R.V., Travin, A.V., Yudin, D.S., Belyatsky, B.V.,
509 2017. Paleozoic tholeiitic magmatism of the Kola province: Spatial distribution,
510 age, and relation to alkaline magmatism. Petrology 25, 42-65.
511 Becker, R.T., Gradstein, F.M., Hammer, O., 2012. Chapter 22 - The Devonian Period,
512 in: Gradstein, F.M., Ogg, J.G., Schmitz, M.D., Ogg, G.M. (Eds.), The Geologic
513 Time Scale. Elsevier, Boston, pp. 559-601.
514 Bergquist, B.A., 2017. Mercury, volcanism, and mass extinctions. Proceedings of the
515 National Academy of Sciences 114, 8675-8677.
516 Biester, H., Scholz, C., 1996. Determination of Mercury Binding Forms in
517 Contaminated Soils: Mercury Pyrolysis versus Sequential Extractions.
518 Environmental Science & Technology 31, 233-239.
519 Biswas, A., Blum, J.D., Keeler, G.J., 2008. Mercury storage in surface soils in a central
520 Washington forest and estimated release during the 2001 Rex Creek Fire. Science
521 of The Total Environment 404, 129-138.
522 Biswas, A., Blum, J.D., Klaue, B., Keeler, G.J., 2007. Release of mercury from Rocky
523 Mountain forest fires. Global Biogeochemical Cycles 21.
524 Bond, D., Wignall, P.B., Racki, G., 2004. Extent and duration of marine anoxia during
525 the Frasnian–Famennian (Late Devonian) mass extinction in Poland, Germany,
526 Austria and France. Geological Magazine 141, 173-193.
527 Bond, D.P.G., Wignall, P.B., 2008. The role of sea-level change and marine anoxia in
528 the Frasnian–Famennian (Late Devonian) mass extinction. Palaeogeography,
529 Palaeoclimatology, Palaeoecology 263, 107-118.
530 Boudinot, F.G., Sepúlveda, J., 2020. Marine organic carbon burial increased forest fire
531 frequency during Oceanic Anoxic Event 2. Nature Geoscience 13, 693-698.
532 Burgess, S. D., Muirhead, J. D., and Bowring, S. A., 2017, Initial pulse of Siberian
533 Traps sills as the trigger of the end-Permian mass extinction: Nature
534 Communications 8, 164.
535 Charbonnier, G., Föllmi, K.B., 2017. Mercury enrichments in lower Aptian sediments
536 support the link between Ontong Java large igneous province activity and oceanic
537 anoxic episode 1a. Geology 45, 63-66.

538 Chester, R., 1990. The transport of material to the oceans: Relative flux magnitudes,
539 Marine Geochemistry. Springer, pp. 149-191.
540 Chen, D., Qing, H., Li, R., 2005. The Late Devonian Frasnian–Famennian (F/F) biotic
541 crisis: Insights from $\delta^{13}C_{carb}$, $\delta^{13}C_{org}$ and $^{87}Sr/^{86}Sr$ isotopic systematics. Earth and
542 Planetary Science Letters 235, 151-166.
543 Claeys, P., Casier, J.-G., Margolis, S.V., 1992. Microtektites and Mass Extinctions:
544 Evidence for a Late Devonian Asteroid Impact. Science 257, 1102-1104.
545 Cohen, A.S., Coe, A.L., 2002. New geochemical evidence for the onset of volcanism
546 in the Central Atlantic magmatic province and environmental change at the
547 Triassic-Jurassic boundary. Geology 30, 267-270.
548 Cohen, A.S., Coe, A.L., Harding, S.M., Schwark, L., 2004. Osmium isotope evidence
549 for the regulation of atmospheric CO_2 by continental weathering. Geology 32,
550 157-160.
551 Courtillot, V., Kravchinsky, V.A., Quidelleur, X., Renne, P.R., Gladkochub, D.P., 2010.
552 Preliminary dating of the Viluy traps (Eastern Siberia): Eruption at the time of
553 Late Devonian extinction events? Earth and Planetary Science Letters 300, 239-
554 245.
555 Da Silva, A.-C., Sinnesael, M., Claeys, P., Davies, J.H.F.L., de Winter, N.J., Percival,
556 L.M.E., Schaltegger, U., De Vleeschouwer, D., 2020. Anchoring the Late
557 Devonian mass extinction in absolute time by integrating climatic controls and
558 radio-isotopic dating. Scientific Reports 10, 12940.
559 Davies, J.H.F.L., Marzoli, A., Bertrand, H., Youbi, N., Ernesto, M., Schaltegger, U.,
560 2017. End-Triassic mass extinction started by intrusive CAMP activity. Nature
561 Communications 8, 15596.
562 Day, J., Witzke, B.J., 2017. Chapter Six - Upper Devonian Biostratigraphy, Event
563 Stratigraphy, and Late Frasnian Kellwasser Extinction Bioevents in the Iowa
564 Basin: Western Euramerica, in: Montenari, M. (Ed.), Stratigraphy & Timescales.
565 Academic Press, pp. 243-332.
566 De Vleeschouwer, D., Da Silva, A.-C., Sinnesael, M., Chen, D., Day, J.E., Whalen,
567 M.T., Guo, Z., Claeys, P., 2017. Timing and pacing of the Late Devonian mass
568 extinction event regulated by eccentricity and obliquity. Nature Communications
569 8, 2268.
570 DeBano, L.F., 2000. The role of fire and soil heating on water repellency in wildland
571 environments: a review. Journal of Hydrology 231-232, 195-206.
572 Dickson, A.J., Cohen, A.S., Coe, A.L., Davies, M., Shcherbinina, E.A., Gavrilov, Y.O.,
573 2015. Evidence for weathering and volcanism during the PETM from Arctic
574 Ocean and Peri-Tethys osmium isotope records. Palaeogeography,
575 Palaeoclimatology, Palaeoecology 438, 300-307.
576 Driscoll, C.T., Mason, R.P., Chan, H.M., Jacob, D.J., Pirrone, N., 2013. Mercury as a
577 Global Pollutant: Sources, Pathways, and Effects. Environmental Science &
578 Technology 47, 4967-4983.

579 Du Vivier, A.D.C., Selby, D., Sageman, B.B., Jarvis, I., Gröcke, D.R., Voigt, S., 2014.
580 Marine $^{187}Os/^{188}Os$ isotope stratigraphy reveals the interaction of volcanism and
581 ocean circulation during Oceanic Anoxic Event 2. Earth and Planetary Science
582 Letters 389, 23-33.
583 Du Vivier, A.D.C., Selby, D., Condon, D.J., Takashima, R., Nishi, H., 2015. Pacific
584 $^{187}Os/^{188}Os$ isotope chemistry and U–Pb geochronology: Synchroneity of global
585 Os isotope change across OAE 2. Earth and Planetary Science Letters 428, 204-
586 216.
587 Estrada, L., Pippenger, K., Boyer, D.L., Jones, D.S., Cohen, P., 2018. Mercury and
588 microfossil trends during end-Devonian extinction events, GSA Annual Meeting
589 in Indianapolis, Indiana, USA-2018. GSA.
590 Fisher, J.A., Jacob, D.J., Soerensen, A.L., Amos, H.M., Steffen, A., Sunderland, E.M.,
591 2012. Riverine source of Arctic Ocean mercury inferred from atmospheric
592 observations. Nature Geoscience 5, 499-504.
593 Friedli, H.R., Radke, L.F., Prescott, R., Hobbs, P.V., Sinha, P., 2003. Mercury
594 emissions from the August 2001 wildfires in Washington State and an agricultural
595 waste fire in Oregon and atmospheric mercury budget estimates. Global
596 Biogeochemical Cycles 17.
597 Gamboa Ruiz, W.L., Tomiyasu, T., 2015. Distribution of mercury in sediments from
598 Kagoshima Bay, Japan, and its relationship with physical and chemical factors.
599 Environmental Earth Sciences 74, 1175-1188.
600 Gehrke, G.E., Blum, J.D., Meyers, P.A., 2009. The geochemical behavior and isotopic
601 composition of Hg in a mid-Pleistocene western Mediterranean sapropel.
602 Geochimica et Cosmochimica Acta 73, 1651-1665.
603 Georgiev, S.V., Stein, H.J., Hannah, J.L., Henderson, C.M., Algeo, T.J., 2015.
604 Enhanced recycling of organic matter and Os-isotopic evidence for multiple
605 magmatic or meteoritic inputs to the Late Permian Panthalassic Ocean, Opal Creek,
606 Canada. Geochimica et Cosmochimica Acta 150, 192-210.
607 Glasspool, I.J., Scott, A.C., 2010. Phanerozoic concentrations of atmospheric oxygen
608 reconstructed from sedimentary charcoal. Nature Geoscience 3, 627.
609 Gordon, G.W., Rockman, M., Turekian, K.K., Over, J., 2009. Osmium isotopic
610 evidence against an impact at the Frasnian-Famennian boundary. 309, 420-430.
611 Grasby, S.E., Beauchamp, B., Bond, D.P.G., Wignall, P.B., Sanei, H., 2016. Mercury
612 anomalies associated with three extinction events (Capitanian Crisis, Latest
613 Permian Extinction and the Smithian/Spathian Extinction) in NW Pangea.
614 Geological Magazine 153, 285-297.
615 Grasby, S.E., Liu, X., Yin, R., Ernst, R.E., Chen, Z., 2020. Toxic mercury pulses into
616 late Permian terrestrial and marine environments. Geology.
617 Grasby, S.E., Sanei, H., Beauchamp, B., Chen, Z., 2013. Mercury deposition through
618 the Permo–Triassic Biotic Crisis. Chemical Geology 351, 209-216.

Grasby, S.E., Shen, W., Yin, R., Gleason, J.D., Blum, J.D., Lepak, R.F., Hurley, J.P., Beauchamp, B., 2017. Isotopic signatures of mercury contamination in latest Permian oceans. Geology 45, 55-58.

Grasby, S.E., Them, T.R., Chen, Z., Yin, R., Ardakani, O.H., 2019. Mercury as a proxy for volcanic emissions in the geologic record. Earth-Science Reviews 196, 102880.

Huang, C., Joachimski, M.M., Gong, Y., 2018. Did climate changes trigger the Late Devonian Kellwasser Crisis? Evidence from a high-resolution conodont δ18OPO4 record from South China. Earth and Planetary Science Letters 495, 174-184.

Joachimski, M.M., Breisig, S., Buggisch, W., Talent, J.A., Mawson, R., Gereke, M., Morrow, J.R., Day, J., Weddige, K., 2009. Devonian climate and reef evolution: Insights from oxygen isotopes in apatite. Earth and Planetary Science Letters 284, 599-609.

Joachimski, M.M., Buggisch, W., 1993. Anoxic events in the late Frasnian—Causes of the Frasnian-Famennian faunal crisis? Geology 21, 675-678.

Joachimski, M.M., Buggisch, W., 2002. Conodont apatite δ18O signatures indicate climatic cooling as a trigger of the Late Devonian mass extinction. Geology 30, 711-714.

Joachimski, M.M., Pancost, R.D., Freeman, K.H., Ostertag-Henning, C., Buggisch, W., 2002. Carbon isotope geochemistry of the Frasnian–Famennian transition. Palaeogeography, Palaeoclimatology, Palaeoecology 181, 91-109.

Johnson, J.G., Klapper, G., Sandberg, C.A., 1985. Devonian Eustatic Fluctuations in Euramerica. Geological Society of America Bulletin 96, 567-587.

Jones, M.T., Percival, L.M.E., Stokke, E.W., Frieling, J., Mather, T.A., Riber, L., Schubert, B.A., Schultz, B., Tegner, C., Planke, S., Svensen, H.H., 2018. Mercury anomalies across the Palaeocene-Eocene Thermal Maximum. Clim. Past Discuss. 2018, 1-35.

Kaiho, K., Aftabuzzaman, M., Jones, D.S., Tian, L., 2020. Pulsed volcanic combustion events coincident with the end-Permian terrestrial disturbance and the following global crisis. Geology 49, 289-293.

Kaiho, K., Miura, M., Tezuka, M., Hayashi, N., Jones, D.S., Oikawa, K., Casier, J.-G., Fujibayashi, M., Chen, Z.-Q., 2021. Coronene, mercury, and biomarker data support a link between extinction magnitude and volcanic intensity in the Late Devonian. Global and Planetary Change 199, 103452.

Kaiho, K., Oshima, N., Adachi, K., Adachi, Y., Mizukami, T., Fujibayashi, M., Saito, R., 2016. Global climate change driven by soot at the K-Pg boundary as the cause of the mass extinction. Scientific Reports 6, 28427.

Kemp, D.B., Selby, D., Izumi, K., 2020. Direct coupling between carbon release and weathering during the Toarcian oceanic anoxic event. Geology.

Kiselev, A.I., Yarmolyuk, V.V., Egorov, K.N., Chernyshov, R.A., Nikiforov, A.V., 2006. Middle Paleozoic basic magmatism of the northwestern Vilyui Rift: Composition, sources, and geodynamics. Petrology 14, 588-608.

660 Klapper, G., Feist, R., Becker, R.T., House, M.R., 1993. Definition of the Frasnian
661 Famennian Stage Boundary. Episodes 16, 433-441.
662 Kravchinsky, V.A., 2012. Paleozoic large igneous provinces of Northern Eurasia:
663 Correlation with mass extinction events. Global and Planetary Change 86-87, 31-
664 36.
665 Kuroda, J., Hori, R.S., Suzuki, K., Gröcke, D.R., Ohkouchi, N., 2010. Marine osmium
666 isotope record across the Triassic-Jurassic boundary from a Pacific pelagic site.
667 Geology 38, 1095-1098.
668 Lima, A.L.C., Farrington, J.W., Reddy, C.M., 2005. Combustion-Derived Polycyclic
669 Aromatic Hydrocarbons in the Environment—A Review. Environmental
670 Forensics 6, 109-131.
671 Liu, Z., Horton, D.E., Tabor, C., Sageman, B.B., Percival, L.M.E., Gill, B.C., Selby,
672 D., 2019a. Assessing the Contributions of Comet Impact and Volcanism Toward
673 the Climate Perturbations of the Paleocene-Eocene Thermal Maximum.
674 Geophysical Research Letters 46, 14798-14806.
675 Liu, Z., Selby, D., Hackley, P.C., Over, D.J., 2020a. Evidence of wildfires and elevated
676 atmospheric oxygen at the Frasnian−Famennian boundary in New York (USA):
677 Implications for the Late Devonian mass extinction. GSA Bulletin.
678 Liu, Z., Selby, D., Zhang, H., Shen, S., 2020b. Evidence for volcanism and weathering
679 during the Permian-Triassic mass extinction from Meishan (South China) osmium
680 isotope record. Palaeogeography, Palaeoclimatology, Palaeoecology 553, 109790.
681 Liu, Z., Selby, D., Zhang, H., Zheng, Q., Shen, S., Sageman, B.B., Grasby, S.E.,
682 Beauchamp, B., 2019b. Osmium-isotope evidence for volcanism across the
683 Wuchiapingian–Changhsingian boundary interval. Chemical Geology 529,
684 119313.
685 McElwain, J.C., Wade-Murphy, J., Hesselbo, S.P., 2005. Changes in carbon dioxide
686 during an oceanic anoxic event linked to intrusion into Gondwana coals. Nature
687 435, 479-482.
688 Moreno, C., González, F., Sáez, R., Melgarejo, J.C., Suárez-Ruiz, I., 2018. The Upper
689 Devonian Kellwasser event recorded in a regressive sequence from inner shelf to
690 lagoonal pond, Catalan Coastal Ranges, Spain. Sedimentology 65, 2055-2087.
691 Obrist, D., 2007. Atmospheric mercury pollution due to losses of terrestrial carbon
692 pools? Biogeochemistry 85, 119-123.
693 Obrist, D., Kirk, J.L., Zhang, L., Sunderland, E.M., Jiskra, M., Selin, N.E., 2018. A
694 review of global environmental mercury processes in response to human and
695 natural perturbations: Changes of emissions, climate, and land use. Ambio 47,
696 116-140.
697 Outridge, Sanei, H., Stern, Hamilton, Goodarzi, F., 2007. Evidence for Control of
698 Mercury Accumulation Rates in Canadian High Arctic Lake Sediments by
699 Variations of Aquatic Primary Productivity. Environmental Science &
700 Technology 41, 5259-5265.

Over, D.J., 1997. Conodont biostratigraphy of the Java Formation (Upper Devonian) and the Frasnian-Famennian boundary in western New York State, in: Klapper, G., Murphy, M.A., Talent, J.A. (Eds.), Paleozoic Sequence Stratigraphy, Biostratigraphy, and Biogeography: Studies in Honor of J. Granville ("Jess") Johnson. Geological Society of America, pp. 161-177.

Over, D.J., 2002. The Frasnian/Famennian boundary in central and eastern United States. Palaeogeography, Palaeoclimatology, Palaeoecology 181, 153-169.

Paschall, O., Carmichael, S.K., Königshof, P., Waters, J.A., Ta, P.H., Komatsu, T., Dombrowski, A., 2019. The Devonian-Carboniferous boundary in Vietnam: Sustained ocean anoxia with a volcanic trigger for the Hangenberg Crisis? Global and Planetary Change 175, 64-81.

Percival, L.M.E., van Helmond, N.A.G.M., Selby, D., Goderis, S., Claeys, P., 2020. Complex Interactions Between Large Igneous Province Emplacement and Global-Temperature Changes During the Cenomanian-Turonian Oceanic Anoxic Event (OAE 2). Paleoceanography and Paleoclimatology 35, e2020PA004016.

Percival, L.M.E., Cohen, A.S., Davies, M.K., Dickson, A.J., Hesselbo, S.P., Jenkyns, H.C., Leng, M.J., Mather, T.A., Storm, M.S., Xu, W., 2016. Osmium isotope evidence for two pulses of increased continental weathering linked to Early Jurassic volcanism and climate change. Geology 44, 759-762.

Percival, L.M.E., Davies, J.H.F.L., Schaltegger, U., De Vleeschouwer, D., Da Silva, A.C., Föllmi, K.B., 2018a. Precisely dating the Frasnian–Famennian boundary: implications for the cause of the Late Devonian mass extinction. Scientific Reports 8, 9578.

Percival, L.M.E., Jenkyns, H.C., Mather, T.A., Dickson, A.J., Batenburg, S.J., Ruhl, M., Hesselbo, S.P., Barclay, R., Jarvis, I., Robinson, S.A., Woelders, L., 2018b. Does large igneous province volcanism always perturb the mercury cycle? Comparing the records of Oceanic Anoxic Event 2 and the end-Cretaceous to other Mesozoic events. American Journal of Science 318, 799-860.

Percival, L.M.E., Ruhl, M., Hesselbo, S.P., Jenkyns, H.C., Mather, T.A., Whiteside, J.H., 2017. Mercury evidence for pulsed volcanism during the end-Triassic mass extinction. Proceedings of the National Academy of Sciences 114, 7929-7934.

Percival, L.M.E., Selby, D., Bond, D.P.G., Rakociński, M., Racki, G., Marynowski, L., Adatte, T., Spangenberg, J.E., Föllmi, K.B., 2019. Pulses of enhanced continental weathering associated with multiple Late Devonian climate perturbations: Evidence from osmium-isotope compositions. Palaeogeography, Palaeoclimatology, Palaeoecology.

Percival, L.M.E., Witt, M.L.I., Mather, T.A., Hermoso, M., Jenkyns, H.C., Hesselbo, S.P., Al-Suwaidi, A.H., Storm, M.S., Xu, W., Ruhl, M., 2015. Globally enhanced mercury deposition during the end-Pliensbachian extinction and Toarcian OAE: A link to the Karoo–Ferrar Large Igneous Province. Earth and Planetary Science Letters 428, 267-280.

Percival, L.M.E., Marynowski, L., Baudin, F., Goderis, S., De Vleeschouwer, D., Rakociński, M., Narkiewicz, K., Da Silva, A.-C. and Claeys, P., Regional variability in the timing and nature of environmental perturbations during the Frasnian–Famennian mass extinction. (in review)

Peucker-Ehrenbrink, B., Ravizza, G., 2000. The marine osmium isotope record. Terra Nova 12, 205-219.

Peucker-Ehrenbrink, B., Ravizza, G., 2012. Osmium Isotope Stratigraphy, in: Gradstein, F.M., Ogg, J.G., Schmitz, M.D., Ogg, G.M. (Eds.), The Geologic Time Scale. Elsevier, Boston, pp. 145-166.

Racki, G., 2020. A volcanic scenario for the Frasnian–Famennian major biotic crisis and other Late Devonian global changes: More answers than questions? Global and Planetary Change 189, 103174.

Racki, G., Adatte, T., Bond, D.P.G., Keller, G., 2020. Volcanism as a prime cause of mass extinctions: Retrospectives and perspectives, Mass Extinctions, Volcanism, and Impacts: New Developments. Geological Society of America, p. 0.

Racki, G., Königshof, P., Belka, Z., Dopieralska, J., Pisarzowska, A., 2019. Diverse depositional and geochemical signatures of the Frasnian-Famennian global event in western Thailand reveal palaeotethyan vs. Western Australian geotectonic affinities. Journal of Asian Earth Sciences: X 2, 100010.

Racki, G., Racka, M., Matyja, H., Devleeschouwer, X., 2002. The Frasnian/Famennian boundary interval in the South Polish–Moravian shelf basins: integrated event-stratigraphical approach. Palaeogeography, Palaeoclimatology, Palaeoecology 181, 251-297.

Racki, G., Rakociński, M., Marynowski, L., 2018a. Anomalous Upper Devonian mercury enrichments: comparison of Inductively Coupled Plasma – Mass Spectrometry (ICP-MS) and Atomic Absorption Spectrometry (AAS) analytical data. 2018 62.

Racki, G., Rakociński, M., Marynowski, L., Wignall, P.B., 2018b. Mercury enrichments and the Frasnian-Famennian biotic crisis: A volcanic trigger proved? Geology 46, 543-546.

Rakociński, M., Marynowski, L., Pisarzowska, A., Bełdowski, J., Siedlewicz, G., Zatoń, M., Perri, M.C., Spalletta, C., Schönlaub, H.P., 2020. Volcanic related methylmercury poisoning as the possible driver of the end-Devonian Mass Extinction. Scientific Reports 10, 7344.

Sageman, B.B., Murphy, A.E., Werne, J.P., Ver Straeten, C.A., Hollander, D.J., Lyons, T.W., 2003. A tale of shales: the relative roles of production, decomposition, and dilution in the accumulation of organic-rich strata, Middle–Upper Devonian, Appalachian basin. Chemical Geology 195, 229-273.

Sanei, H., Grasby, S.E., Beauchamp, B., 2012. Latest Permian mercury anomalies. Geology 40, 63-66.

Sanei, H., Outridge, P.M., Stern, G.A., Macdonald, R.W., 2014. Classification of mercury–labile organic matter relationships in lake sediments. Chemical Geology 373, 87-92.

Shen, J., Algeo, T.J., Chen, J., Planavsky, N.J., Feng, Q., Yu, J., Liu, J., 2019a. Mercury in marine Ordovician/Silurian boundary sections of South China is sulfide-hosted and non-volcanic in origin. Earth and Planetary Science Letters 511, 130-140.

Shen, J., Chen, J., Algeo, T.J., Yuan, S., Feng, Q., Yu, J., Zhou, L., O'Connell, B., Planavsky, N.J., 2019b. Evidence for a prolonged Permian–Triassic extinction interval from global marine mercury records. Nature Communications 10, 1563.

Shen, J., Yu, J., Chen, J., Algeo, T.J., Xu, G., Feng, Q., Shi, X., Planavsky, N.J., Shu, W., Xie, S., 2019. Mercury evidence of intense volcanic effects on land during the Permian-Triassic transition. Geology 47, 1117-1121.

Shen, J., Feng, Q., Algeo, T.J., Liu, J., Zhou, C., Wei, W., Liu, J., Them, T.R., Gill, B.C., Chen, J., 2020. Sedimentary host phases of mercury (Hg) and implications for use of Hg as a volcanic proxy. Earth and Planetary Science Letters 543, 116333.

Sholupov, S.E., Ganeyev, A.A., 1995. Zeeman atomic absorption spectrometry using high frequency modulated light polarization. Spectrochimica Acta Part B: Atomic Spectroscopy 50, 1227-1236.

Song, Y., Gilleaudeau, G.J., Algeo, T.J., Over, D.J., Lyons, T.W., Anbar, A.D., Xie, S., 2020. Biomarker evidence of algal-microbial community changes linked to redox and salinity variation, Upper Devonian Chattanooga Shale (Tennessee, USA). GSA Bulletin.

Song, H., Song, H., Algeo, T.J., Tong, J., Romaniello, S.J., Zhu, Y., Chu, D., Gong, Y., Anbar, A.D., 2017. Uranium and carbon isotopes document global-ocean redox-productivity relationships linked to cooling during the Frasnian-Famennian mass extinction. Geology 45, 887-890.

Soerensen, A.L., Jacob, D.J., Streets, D.G., Witt, M.L.I., Ebinghaus, R., Mason, R.P., Andersson, M., Sunderland, E.M., 2012. Multi-decadal decline of mercury in the North Atlantic atmosphere explained by changing subsurface seawater concentrations. Geophysical Research Letters 39.

Stanley, S.M., 2016. Estimates of the magnitudes of major marine mass extinctions in earth history. Proc Natl Acad Sci U S A 113, E6325-E6334.

Stephens, N.P., Sumner, D.Y., 2003. Late Devonian carbon isotope stratigraphy and sea level fluctuations, Canning Basin, Western Australia. Palaeogeography, Palaeoclimatology, Palaeoecology 191, 203-219.

Svensen, H., Planke, S., Malthe-Sørenssen, A., Jamtveit, B., Myklebust, R., Rasmussen Eidem, T., Rey, S.S., 2004. Release of methane from a volcanic basin as a mechanism for initial Eocene global warming. Nature 429, 542.

Svensen, H., Planke, S., Polozov, A.G., Schmidbauer, N., Corfu, F., Podladchikov, Y.Y., Jamtveit, B., 2009. Siberian gas venting and the end-Permian environmental crisis. Earth and Planetary Science Letters 277, 490-500.

Them, T.R., Gill, B.C., Selby, D., Gröcke, D.R., Friedman, R.M., Owens, J.D., 2017. Evidence for rapid weathering response to climatic warming during the Toarcian Oceanic Anoxic Event. Scientific Reports 7, 5003.

Them, T.R., Jagoe, C.H., Caruthers, A.H., Gill, B.C., Grasby, S.E., Gröcke, D.R., Yin, R., Owens, J.D., 2019. Terrestrial sources as the primary delivery mechanism of mercury to the oceans across the Toarcian Oceanic Anoxic Event (Early Jurassic). Earth and Planetary Science Letters 507, 62-72.

Turgeon, S.C., Creaser, R.A., 2008. Cretaceous oceanic anoxic event 2 triggered by a massive magmatic episode. Nature 454, 323-326.

Turgeon, S.C., Creaser, R.A., Algeo, T.J., 2007. Re–Os depositional ages and seawater Os estimates for the Frasnian–Famennian boundary: Implications for weathering rates, land plant evolution, and extinction mechanisms. Earth and Planetary Science Letters 261, 649-661.

Wang, K., Geldsetzer, H.H.J., Goodfellow, W.D., Krouse, H.R., 1996. Carbon and sulfur isotope anomalies across the Frasnian-Famennian extinction boundary, Alberta, Canada. Geology 24, 187-191.

Webster, J.P., Kane, T.J., Obrist, D., Ryan, J.N., Aiken, G.R., 2016. Estimating mercury emissions resulting from wildfire in forests of the Western United States. Science of The Total Environment 568, 578-586.

Woodruff, L.G., Cannon, W.F., 2010. Immediate and Long-Term Fire Effects on Total Mercury in Forests Soils of Northeastern Minnesota. Environmental Science & Technology 44, 5371-5376.

Wieczorek, R., Fantle, M.S., Kump, L.R., Ravizza, G., 2013. Geochemical evidence for volcanic activity prior to and enhanced terrestrial weathering during the Paleocene Eocene Thermal Maximum. Geochimica et Cosmochimica Acta 119, 391-410.

List of figures:

Figure 1. Reconstructed paleogeography map showing location of the Appalachian Basin (open square) and Illinois Basin (red circle) in North America, after Joachimski et al. (2009). Inserted map showing present day New York sample locations – 1: Walnut Creek Bank, 2: Irish Gulf, 3: West Valley, 4: Beaver Meadow Creek, 5: Joint Creek).

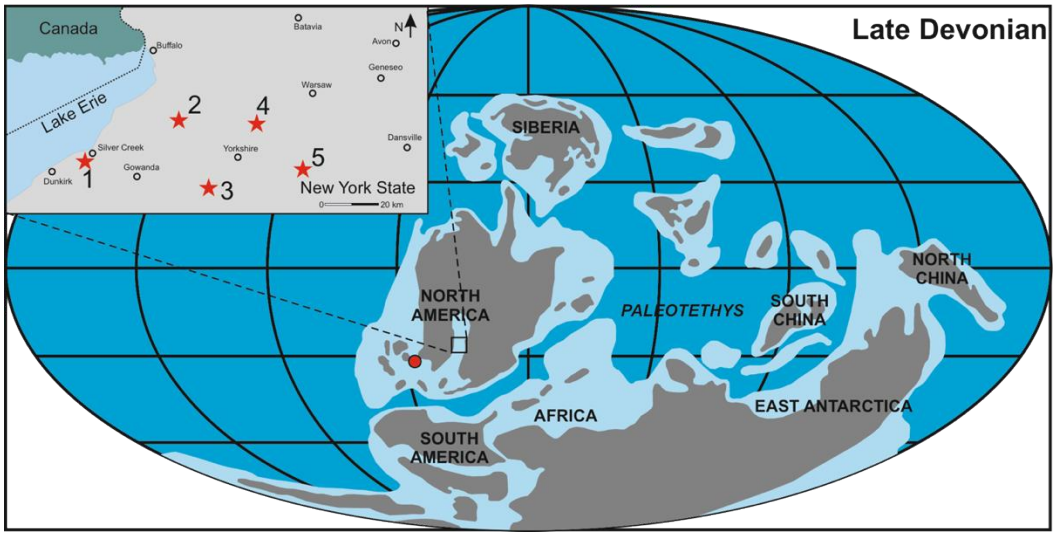

Figure 2. Hg and Hg/TOC stratigraphy for the New York sections investigated. Inertinite data (volume percentage), Mo abundance and TOC data are from Liu et al. (2020a).

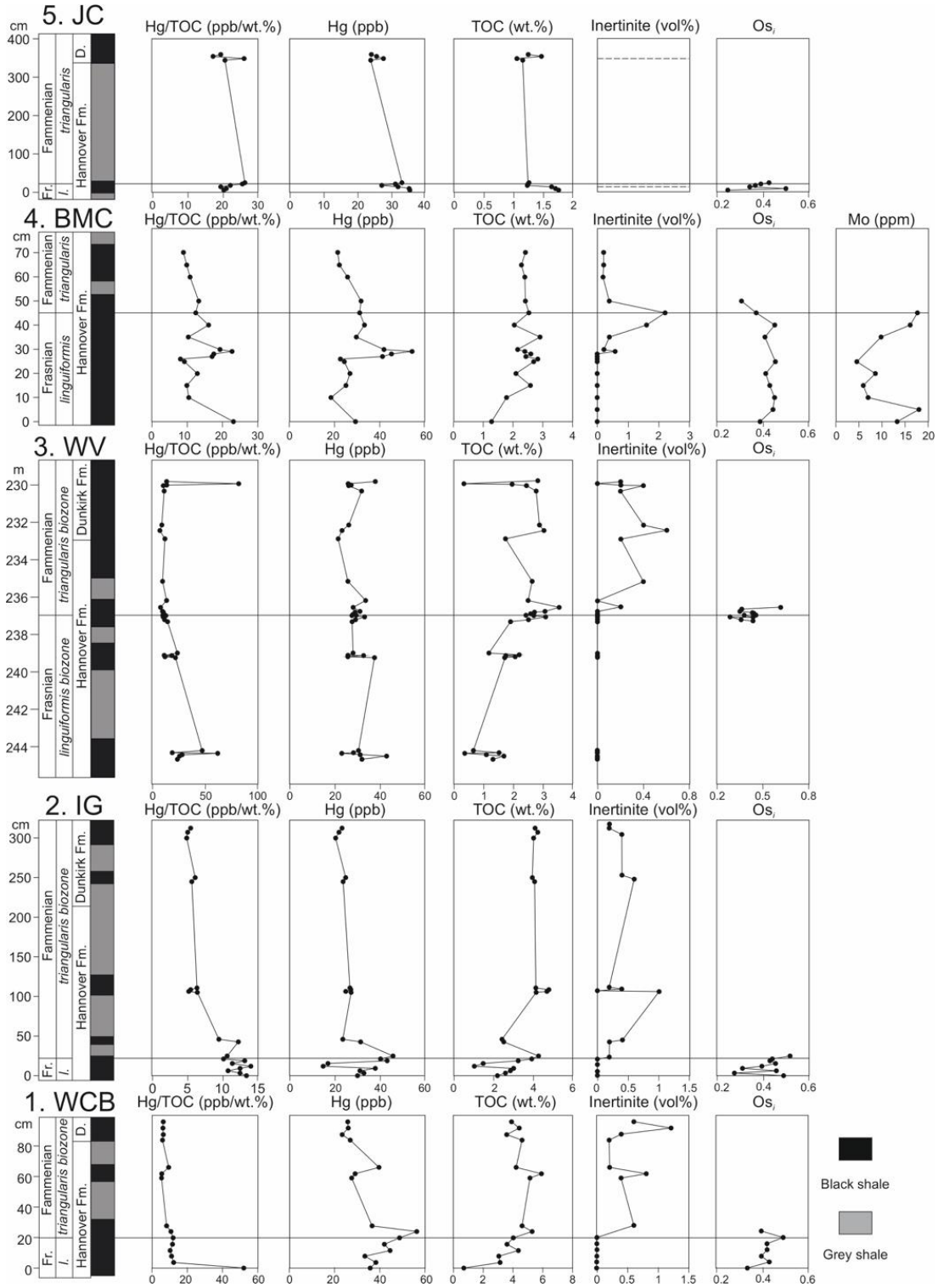

859 **Figure 3.** Stratigraphic plot of $^{13}C_{org}$, Hg and Hg/TOC data for the H-32 section. $^{13}C_{org}$

860 and TOC data are from Percival et al. (in review).

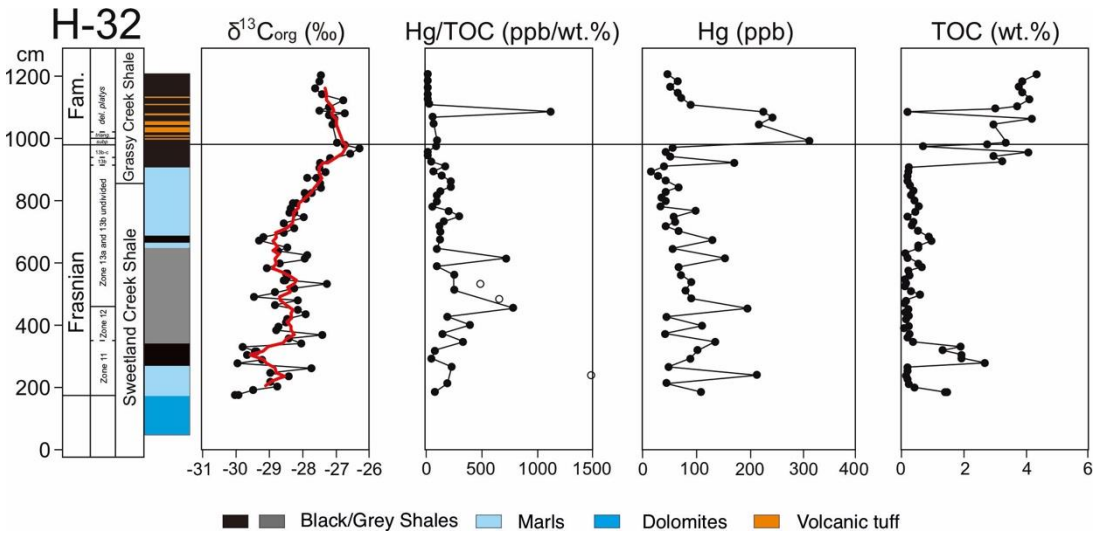

861

862 **Figure 4.** Crossplots of Hg and Hg/TOC with TOC, Al_2O_3, Mo, Mn, V/(V+Ni) and

863 Si/Al.

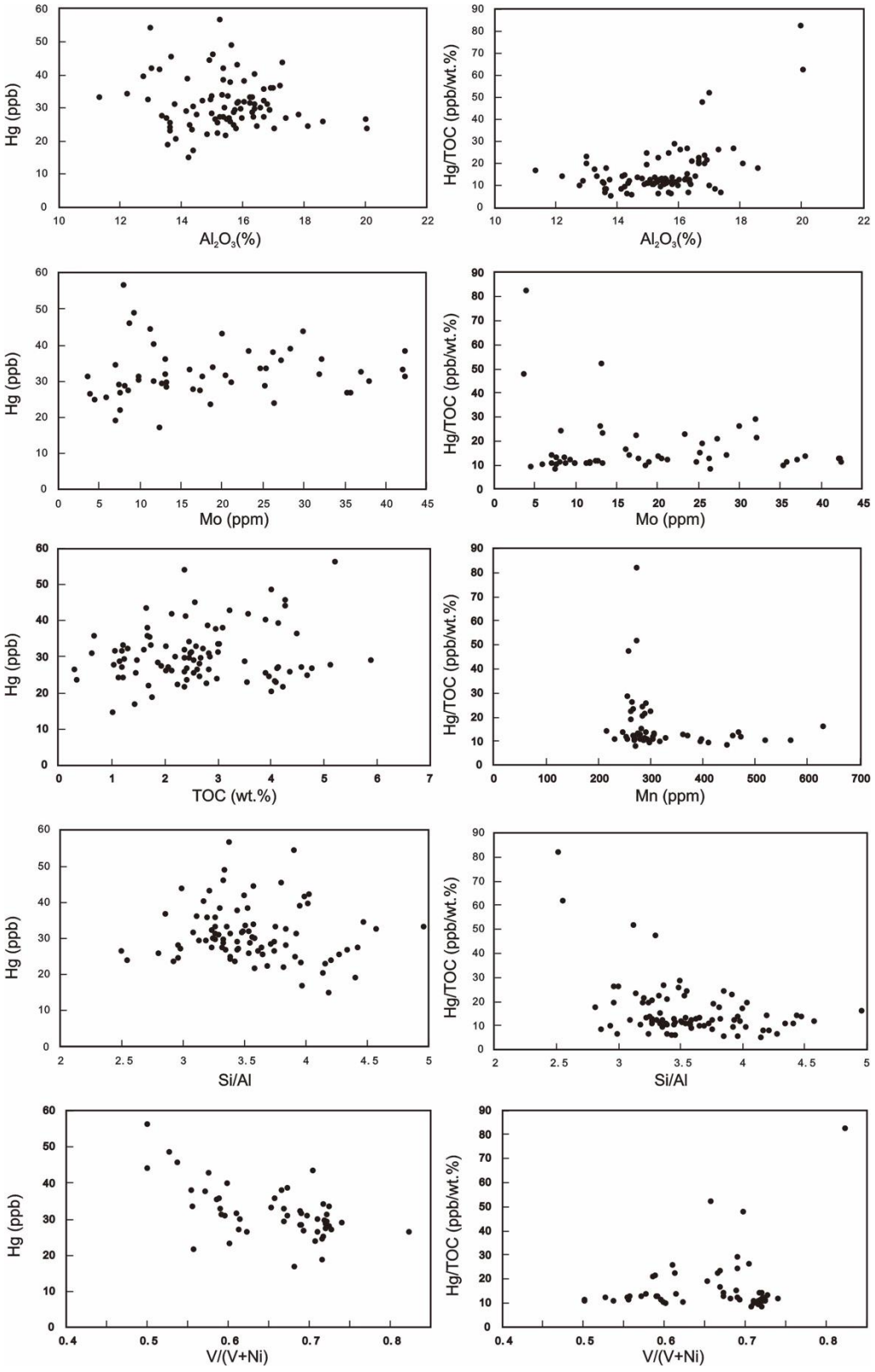

864